

Structural and Spectroscopic Features of a *cis* (Hydroxo)-Fe^{III}-(Carboxylato) Configuration as an Active Site Model for Lipoxygenases

Seiji Ogo,^{*,†,‡} Ryo Yamahara,^{†,§} Mark Roach,[†] Tomoyoshi Suenobu,[†] Michihiko Aki,[†] Takashi Ogura,^{||} Teizo Kitagawa,^{†,⊥} Hideki Masuda,[§] Shunichi Fukuzumi,^{*,†} and Yoshihito Watanabe^{*,†,⊥,∇}

Department of Material and Life Science, Graduate School of Engineering, Osaka University, PRESTO & CREST, Japan Science and Technology Corporation (JST), Suita, Osaka 565-0871, Japan, Institute for Molecular Science, Myodaiji, Okazaki 444-8585, Japan, Nagoya Institute of Technology, Gokiso-cho, Showa-ku, Nagoya 466-8555, Japan, Department of Life Sciences, Graduate School of Arts and Sciences, The University of Tokyo, Komaba, Meguro-ku, Tokyo 153-8902, Japan, Center for Integrative Bioscience, Myodaiji, Okazaki 444-8585, Japan, and Department of Chemistry, Graduate School of Science, Nagoya University, Chikusa-ku, Nagoya 464-8602, Japan

Received January 2, 2002

In our preliminary communication (Ogo, S.; Wada, S.; Watanabe, Y.; Iwase, M.; Wada, A.; Harata, M.; Jitsukawa, K.; Masuda, H.; Einaga, H. *Angew. Chem., Int. Ed.* **1998**, *37*, 2102–2104), we reported the first example of X-ray analysis of a mononuclear six-coordinate (hydroxo)iron(III) non-heme complex, [Fe^{III}(tnpa)(OH)(RCO₂)]ClO₄ [tnpa = tris(6-neopentylamino-2-pyridylmethyl)amine; for **1**, R = C₆H₅], which has a characteristic *cis* (hydroxo)-Fe^{III}-(carboxylato) configuration that models the *cis* (hydroxo)-Fe^{III}-(carboxylato) moiety of the proposed (hydroxo)-iron(III) species of lipoxygenases. In this full account, we report structural and spectroscopic characterization of the *cis* (hydroxo)-Fe^{III}-(carboxylato) configuration by extending the model complexes from **1** to [Fe^{III}(tnpa)(OH)(RCO₂)]ClO₄ (**2**, R = CH₃; **3**, R = H) whose *cis* (hydroxo)-Fe^{III}-(carboxylato) moieties are isotopically labeled by ¹⁸OH⁻, ¹⁶OD⁻, ¹⁸OD⁻, ¹²CH₃¹²C¹⁸O₂⁻, ¹²CH₃¹³C¹⁶O₂⁻, ¹³CH₃¹²C¹⁶O₂⁻, ¹³CH₃¹³C¹⁶O₂⁻, and H¹³C¹⁶O₂⁻. Complexes **1–3** are characterized by X-ray analysis, IR, EPR, and UV–vis spectroscopy, and electrospray ionization mass spectrometry (ESI-MS).

Introduction

Mononuclear non-heme iron enzymes, lipoxygenases (LOs), which are found in plants and in animals, catalyze the peroxidation of polyunsaturated fatty acids containing the *cis,cis*-1,4-diene moiety to the corresponding 1-hydroperoxy-*trans,cis*-2,4-diene.¹ To date, two kinds of crystal structures of catalytically inactive iron(II) species of a plant LO (soybean lipoxygenase-1, SLO-1)² and a mammalian LO (15-rabbit lipoxygenase, 15-RLO)³ have been reported. The crystal structure of the plant LO (SLO-1) at 1.4 Å resolution

(Figure 1a)^{2a} has revealed that the iron(II) core structure has six-coordinate octahedral geometry with one carboxylato from the C-terminal isoleucine (Ile839), one carboxyamido carbonyl oxygen atom from the asparagine (Asn694) which is weakly associated with the iron atom (Fe···O = 3.05 Å),

* To whom correspondence should be addressed. E-mail: ogo@chem.eng.osaka-u.ac.jp (S.O.).

† Osaka University, PRESTO & CREST (JST).

‡ Institute for Molecular Science.

§ Nagoya Institute of Technology.

|| The University of Tokyo.

⊥ Center for Integrative Bioscience.

∇ Nagoya University.

- (1) Reviews: (a) Solomon, E. I.; Brunold, T. C.; Davis, M. I.; Kemsley, J. N.; Lee, S.-K.; Lehnert, N.; Neese, F.; Skulan, A. J.; Yang, Y.-S.; Zhou, J. *Chem. Rev.* **2000**, *100*, 235–349. (b) Funabiki, T. In *Oxygenases and Model Systems*; Funabiki, T., Ed.; Kluwer Academic Publishers: Dordrecht, The Netherlands, 1997; pp 69–77 and 140–145. (c) Que, L., Jr.; Ho, R. Y. N. *Chem. Rev.* **1996**, *96*, 2607–2624. (d) Nelson, M. J.; Seitz, S. P. In *Active Oxygen in Biochemistry*; Valentine, J. S., Foote, C. S., Greenberg, A., Liebman, J. F., Eds.; Chapman & Hall: London, 1995; pp 276–312.
- (2) (a) Minor, W.; Steczko, J.; Stec, B.; Otwinowski, Z.; Bolin, J. T.; Walter, R.; Axelrod, B. *Biochemistry* **1996**, *35*, 10687–10701. (b) Minor, W.; Steczko, J.; Bolin, J. T.; Otwinowski, Z.; Axelrod, B. *Biochemistry* **1993**, *32*, 6320–6323.
- (3) (a) Gillmor, S. A.; Villaseñor, A.; Fletterick, R.; Sigal, E.; Browner, M. F. *Nat. Struct. Biol.* **1997**, *4*, 1003–1009. (b) Boyington, J. C.; Gaffney, B. J.; Amzel, L. M. *Science* **1993**, *260*, 1482–1486.

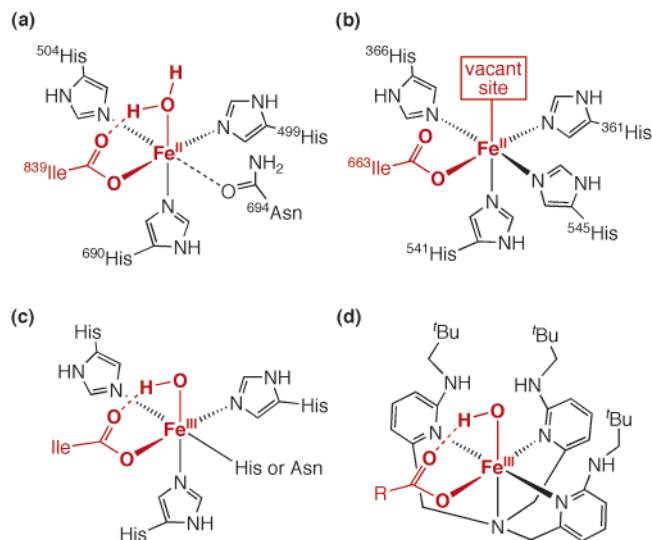


Figure 1. Core structure of catalytically inactive iron(II) species determined by X-ray analysis of (a) a plant lipoxygenase (soybean lipoxygenase-1, SLO-1) and (b) a mammalian lipoxygenase (15-rabbit lipoxygenase, 15-RLO). (c) Proposed core structure of the catalytically active species of SLO-1 or 15-RLO. (d) Cation of model complexes $[\text{Fe}^{\text{III}}(\text{tnpa})(\text{OH})(\text{RCO}_2)]\text{ClO}_4$ (**1**, $\text{R} = \text{C}_6\text{H}_5$; **2**, $\text{R} = \text{CH}_3$; **3**, $\text{R} = \text{H}$). Dashed line represents an intramolecular hydrogen bond.

three imidazoles from the histidines (His499, His504, and His690), and one water molecule (which forms an intramolecular hydrogen bond with Ile839). On the other hand, the crystal structure of the mammalian LO (15-RLO) at 2.4 Å resolution (Figure 1b)^{3a} has revealed that the iron(II) core structure also has octahedral coordination geometry with one carboxylato from the C-terminal isoleucine (Ile663), four imidazoles from the histidines (His361, His366, His541, and His545), and one vacant coordination site capable of accommodating an exogenous ligand such as a water molecule. In addition, very recently, a crystal structure of the (alkylperoxo)iron(III) species of soybean lipoxygenase-3 was determined by X-ray analysis.⁴

On the basis of the preceding X-ray analysis and various spectroscopic studies,⁵ it is proposed that the catalytically active species of the plant and mammalian LOs adopt six-coordinate iron(III) core structures with the five protein ligands identified in the crystal structures and one hydroxo ligand (Figure 1c).¹ Interestingly, the proposed active sites of the plant and mammalian LOs share a characteristic *cis* (hydroxo)- Fe^{III} -(carboxylato) configuration. It is generally accepted that the functional role of the hydroxo ligand is to

abstract a C-3 hydrogen of the *cis,cis*-1,4-diene to initiate the catalytic reaction,¹ but the functional role of the carboxylato ligand has not been understood. It is thus of importance to characterize the *cis* (hydroxo)- Fe^{III} -(carboxylato) configuration.

There are, however, a few examples of X-ray analysis and infrared (IR) and Raman spectroscopic characterization of mononuclear six-coordinate (hydroxo)iron(III) species of non-heme iron complexes compared with those of heme iron complexes. In the studies of LOs, IR and Raman spectroscopic characterization of the (hydroxo)iron(III) species have not been reported because it is very hard to do IR and Raman at good resolution on the enzyme, while only vibrational frequencies and band assignments for catechol-bound iron(III) species of SLO-1 have been reported.⁶ In our preliminary communication,⁷ we reported a crystal structure of a model complex for the proposed (hydroxo)iron(III) species of lipoxygenases, $[\text{Fe}^{\text{III}}(\text{tnpa})(\text{OH})(\text{RCO}_2)]\text{ClO}_4$ [$\text{tnpa} = \text{tris}(6\text{-neopentylamino-2-pyridylmethyl})\text{amine}$; for **1**, $\text{R} = \text{C}_6\text{H}_5$, Figure 1d], which has the characteristic *cis* (hydroxo)- Fe^{III} -(carboxylato) configuration.

Herein, we report structural and spectroscopic characterization of the *cis* (hydroxo)- Fe^{III} -(carboxylato) configuration by extending the model complexes from **1** to $[\text{Fe}^{\text{III}}(\text{tnpa})(\text{OH})(\text{RCO}_2)]\text{ClO}_4$ (**2**, $\text{R} = \text{CH}_3$; **3**, $\text{R} = \text{H}$, Figure 1d) whose *cis* (hydroxo)- Fe^{III} -(carboxylato) moieties are isotopically labeled by $^{18}\text{OH}^-$, $^{16}\text{OD}^-$, $^{18}\text{OD}^-$, $^{12}\text{CH}_3^{12}\text{C}^{18}\text{O}_2^-$, $^{12}\text{CH}_3^{13}\text{C}^{16}\text{O}_2^-$, $^{13}\text{CH}_3^{12}\text{C}^{16}\text{O}_2^-$, $^{13}\text{CH}_3^{13}\text{C}^{16}\text{O}_2^-$, and $\text{H}^{13}\text{C}^{16}\text{O}_2^-$. Complexes **1–3** are characterized by X-ray analysis, IR, EPR, and UV-vis spectroscopy, and electrospray ionization mass spectrometry (ESI-MS).

Results and Discussion

Synthesis of the Ligand and Complexes. The tetradentate tripodal ligand *tnpa* was designed and synthesized to mimic specific attributes of a proposed (hydroxo)iron(III) species of lipoxygenases (Figure 1c), which has a 4-coordinate environment (one tertiary amine and three pyridine subunits) which can accommodate the fifth and sixth exogenous ligands (e.g., carboxylato and hydroxo). Complexes **1–3** were synthesized by a reaction of $\text{Fe}(\text{ClO}_4)_3 \cdot x\text{H}_2\text{O}$ with an equimolar amount of *tnpa* and RCO_2Na (**1**, $\text{R} = \text{C}_6\text{H}_5$; **2**, $\text{R} = \text{CH}_3$; **3**, $\text{R} = \text{H}$) in acetonitrile containing a small amount of H_2O (see Experimental Section). Complexes **1–3** are stable for months under air at ambient temperature.

Crystal Structures. Structures of **1**⁷ and **2**⁸ were determined by X-ray analysis. An ORTEP drawing of **2** is shown in Figure 2. Complexes **1** and **2** adopt a distorted octahedral coordination which is surrounded by the tetradentate tripodal *tnpa*, monodentate RCO_2^- (**1**, $\text{R} = \text{C}_6\text{H}_5$; **2**, $\text{R} = \text{CH}_3$), and

(4) Skrzypczak-Jankun, E.; Bross, R. A.; Carroll, R. T.; Dunhan, W. R.; Funk, M. O., Jr. *J. Am. Chem. Soc.* **2001**, *123*, 10814–10820.

(5) (a) Scarrow, R. C.; Trimitsis, M. G.; Buck, C. P.; Grove, G. N.; Cowling, R. A.; Nelson, M. J. *Biochemistry* **1994**, *33*, 15023–15035. (b) Navaratnam, S.; Feiters, M. C.; Al-Hakim, M.; Allen, J. C.; Veldink, G. A.; Vliegthart, J. F. G. *Biochim. Biophys. Acta* **1988**, *956*, 70–76. (c) Slappendel, S.; Veldink, G. A.; Vliegthart, J. F. G.; Aasa, R.; Malmström, B. G. *Biochim. Biophys. Acta* **1981**, *667*, 77–86. (d) Slappendel, S.; Veldink, G. A.; Vliegthart, J. F. G.; Aasa, R.; Malmström, B. G. *Biochim. Biophys. Acta* **1980**, *642*, 30–39. (e) Pistorius, E. K.; Axelrod, B.; Palmer, G. *J. Biol. Chem.* **1976**, *251*, 7144–7148. (f) Pavlosky, M. A.; Zhang, Y.; Westre, T. E.; Gan, Q.-F.; Pavel, E. G.; Campochiaro, C.; Hedman, B.; Hodgson, K. O.; Solomon, E. I. *J. Am. Chem. Soc.* **1995**, *117*, 4316–4327. (g) Pavlosky, M. A.; Solomon, E. I. *J. Am. Chem. Soc.* **1994**, *116*, 11610–11611. (h) Whittaker, J. W.; Solomon, E. I. *J. Am. Chem. Soc.* **1988**, *110*, 5329–5339.

(6) Nelson, M. J.; Brennan, B. A.; Chase, D. B.; Cowling, R. A.; Grove, G. N.; Scarrow, R. C. *Biochemistry* **1995**, *34*, 15219–15229.

(7) Ogo, S.; Wada, S.; Watanabe, Y.; Iwase, M.; Wada, A.; Harata, M.; Jitsukawa, K.; Masuda, H.; Einaga, H. *Angew. Chem., Int. Ed.* **1998**, *37*, 2102–2104.

(8) Crystal data for **2**: $\text{C}_{35}\text{H}_{55}\text{ClFeN}_7\text{O}_7$, MW 777.16, monoclinic, space group $P2_1/c$ (No. 14), $a = 13.664(3)$ Å, $b = 16.419(3)$ Å, $c = 18.5181(9)$ Å, $\beta = 93.885(1)^\circ$, $V = 4144(1)$ Å³, $Z = 4$, $D_c = 1.245$ g cm⁻³, $\mu(\text{Mo K}\alpha) = 4.79$ cm⁻¹, $R = 0.072$, and $R_w = 0.173$.

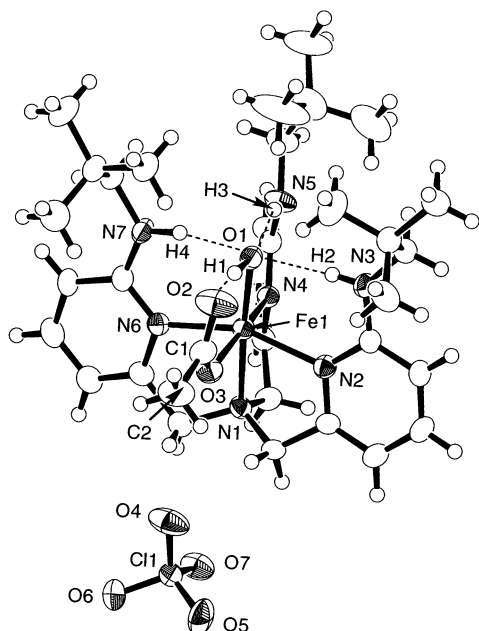


Figure 2. ORTEP drawing of **2**. Selected bond lengths (Å) and angles (deg) as well as interatomic distance (Å): Fe1–O1 = 1.872(3), Fe1–O3 = 1.998(3), Fe1–N1 = 2.150(3), Fe1–N2 = 2.172(3), Fe1–N4 = 2.201(3), Fe1–N6 = 2.164(3), Fe1–O2 = 3.231(3), O2–C1 = 1.236(5), O3–C1 = 1.278(5), C1–C2 = 1.500(6), O1–H1 = 1.03, O(1)–H(2) = 1.99, O(1)–H(3) = 2.08, O(1)–H(4) = 1.87, O(2)–H(1) = 1.61, N3–H2 = 0.84, N5–H3 = 0.75, N7–H4 = 1.00; O2–C1–O3 = 124.7(4), Fe1–O1–H1 = 93.0, O1–H1–O2 = 171.1, O1–H2–N3 = 172.0, O1–H3–N5 = 161.4, O1–H4–N7 = 160.4.

OH[−] ligands. The Fe–OH bond lengths of **1** [1.876(2) Å] and **2** [1.872(3) Å] agree well with that of the ferric SLO-1 as established by EXAFS (1.88 Å). Complexes **1** and **2** have a *cis*-configuration between the OH[−] ligand and the RCO₂[−] or three NH ligands of tnpa to form four intramolecular hydrogen bonds, for example, for **2**, O(1)–H(2) = 1.99 Å, O(1)–H(3) = 2.08 Å, O(1)–H(4) = 1.87 Å, and O(2)–H(1) = 1.61 Å. These hydrogen bonds may contribute to the stabilization of the (hydroxo)iron(III) core structures of **1** and **2**. Moreover, the steric bulk of the neopentylamino groups of tnpa prevents the complex from polymerization, and thus, these groups are required to form the stable (hydroxo)iron(III) complexes. Recently, Borovik et al.⁹ have reported crystal structures of mononuclear five-coordinate (oxo)iron(III) [Fe–O_{oxo} = 1.813(3) Å] and (hydroxo)iron(II) [Fe–O_{hydroxo} = 2.048(3) Å] complexes with a supporting ligand that is similar to that employed in this study. These complexes have the NH⋯OH hydrogen bonds that may reduce the Lewis basicity of the oxygen atom of the hydroxo group. In contrast, the RCOO⋯HO hydrogen bonds in **1** and **2** may increase the Lewis basicity of the oxygen atom of the hydroxo group.

Isotopic Labeling Experiments. We have utilized CH₃COO[−] and HCOO[−] as the carboxylato ligands because of the easily available isotopomers (**2**, ¹²CH₃¹²C¹⁸O₂[−], ¹²CH₃¹³C¹⁶O₂[−], ¹³CH₃¹²C¹⁶O₂[−], and ¹³CH₃¹³C¹⁶O₂[−] for

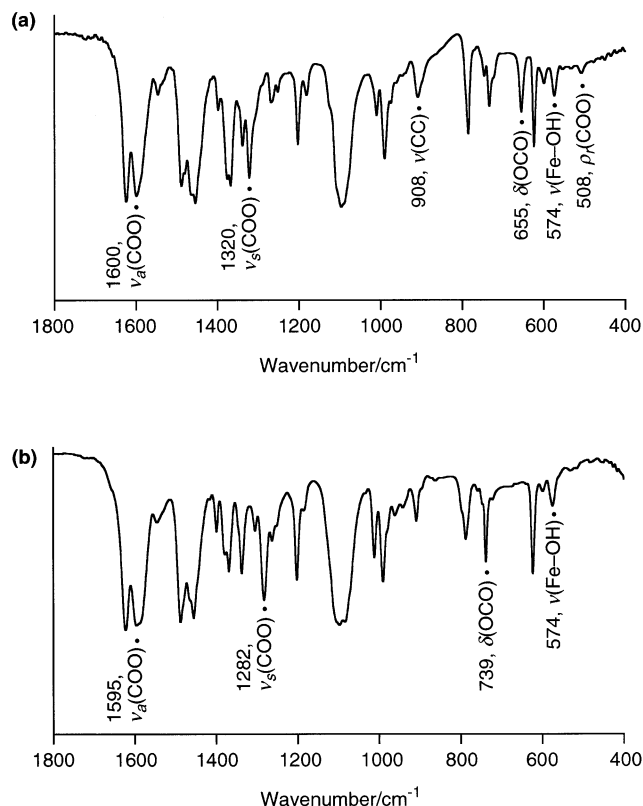


Figure 3. IR spectra in the 400–1800 cm^{−1} region in mineral oil of (a) **2** and (b) **3**.

Table 1. IR Vibrations of Free Acetate and Formate Ions and Acetato and Formato Ligands of **2** and **3** in the Solid State (cm^{−1})^a

	$\nu_a(\text{COO})$	$\nu_s(\text{COO})$	$\nu(\text{CC})$	$\delta(\text{OCO})$	$\rho_t(\text{COO})$
CH ₃ COO [−] (Na salt) ^b	1578	1414	924	646	460
HCOO [−] (Na salt) ^b	1567	1366		772	
2 with CH ₃ COO [−]	1600	1320	908	655	508
2 with CH ₃ C ¹⁸ O ¹⁸ O [−]	1596	1307	911	624	491
2 with CH ₃ ¹³ COO [−]	1597	1297	905	655	505
2 with ¹³ CH ₃ COO [−]	1600	1320	900	649	506
2 with ¹³ CH ₃ ¹³ COO [−]	1597	1297	896	648	503
3 with HCOO [−]	1595	1282		739	
3 with H ¹³ COO [−]	1544	1261		732	

^a Abbreviations used: ν = stretching, δ = deformation, ρ_t = rocking. Subscript a and s denote antisymmetric and symmetric, respectively. ^b Ref 10.

Table 2. Fe^{III}–OH Stretching Frequencies of **2** and **3** in the Solid State (in Mineral Oil) and in the Liquid (in Acetonitrile) State (cm^{−1})

	mineral oil	acetonitrile
2 with OH [−]	574	574
2 with ¹⁸ OH [−]	554	554
2 with OD [−]	574	574
2 with ¹⁸ OD [−]	554	554
3 with OH [−]	574	574
3 with ¹⁸ OH [−]	554	554
3 with OD [−]	574	574
3 with ¹⁸ OD [−]	554	554

¹²CH₃¹²C¹⁶O₂[−]; **3**, H¹³C¹⁶O₂[−] for H¹²C¹⁶O₂[−]). The IR frequencies and band assignments for the *cis* (hydroxo)-Fe^{III}-(carboxylato) moieties of **2** and **3** are summarized in Tables 1 and 2 and Figure 3. The isotopic compositions of the *cis* (hydroxo)-Fe^{III}-(carboxylato) moieties are depicted to the right of each IR spectrum in the figures. It was confirmed by ESI-MS that the structures of the isotopically labeled

(9) (a) MacBeth, C. E.; Golombek, A. P.; Young, V. G., Jr.; Yang, C.; Kuczera, K.; Hendrich, M. P.; Borovik, A. S. *Science* **2000**, *289*, 938–941. (b) MacBeth, C. E.; Hammes, B. S.; Young, V. G., Jr.; Borovik, A. S. *Inorg. Chem.* **2001**, *40*, 4733–4741.

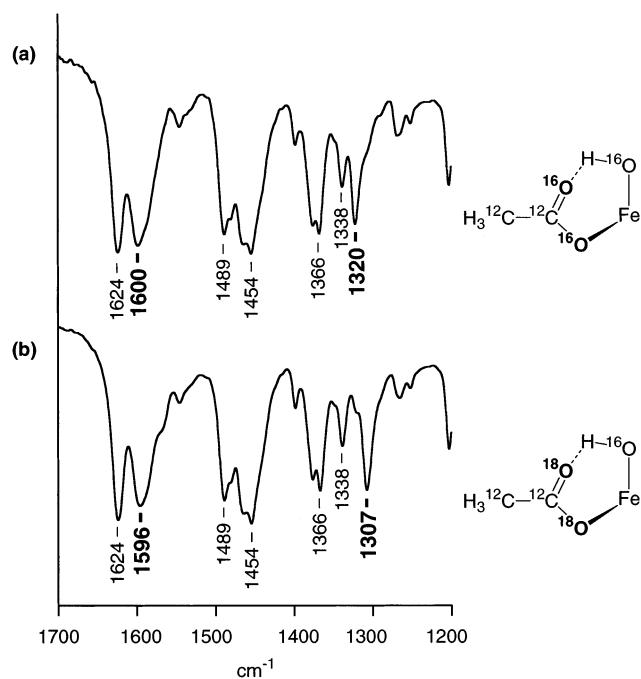


Figure 4. IR spectra in the 1200–1700 cm^{-1} region in mineral oil of (a) **2** with $^{12}\text{CH}_3^{12}\text{C}^{16}\text{O}_2^-$ and (b) **2** with $^{12}\text{CH}_3^{12}\text{C}^{18}\text{O}_2^-$.

complexes are preserved in acetonitrile under the same conditions of IR experiments in acetonitrile. In addition, it was confirmed that the peak at 624 cm^{-1} observed in all of the IR spectra is due to the counteranion ClO_4^- .

IR Spectra of COO Stretching. It is known that free CH_3COO^- and HCOO^- exhibit the antisymmetric COO stretching frequencies, $\nu_a(\text{COO})$, at 1578 and 1567 cm^{-1} , respectively, and the symmetric COO stretching frequencies, $\nu_s(\text{COO})$, at 1414 and 1366 cm^{-1} , respectively (Table 1).¹⁰ In general, if the carboxylato ions bind to a metal ion as monodentate ligands, the $\nu_a(\text{COO})$ and $\nu_s(\text{COO})$ shift to higher and lower frequencies, respectively. Figure 4 shows the IR spectra in mineral oil in the range 1200–1700 cm^{-1} of **2** with $^{12}\text{CH}_3^{12}\text{C}^{16}\text{O}_2^-$ (spectrum a) and $^{12}\text{CH}_3^{12}\text{C}^{18}\text{O}_2^-$ (spectrum b) ligands. The peaks at 1600 and 1320 cm^{-1} (in spectrum a) were assigned to $\nu_a(\text{COO})$ and $\nu_s(\text{COO})$, respectively, because they shift to 1596 and 1307 cm^{-1} (in spectrum b), respectively, by isotopic substitution of $^{12}\text{CH}_3^{12}\text{C}^{18}\text{O}_2^-$ for $^{12}\text{CH}_3^{12}\text{C}^{16}\text{O}_2^-$. Figure S1 (in Supporting Information) shows the IR spectra of $^{12}\text{CH}_3^{13}\text{C}^{16}\text{O}_2^-$, $^{13}\text{CH}_3^{12}\text{C}^{16}\text{O}_2^-$, and $^{13}\text{CH}_3^{13}\text{C}^{16}\text{O}_2^-$ derivatives of **2** in mineral oil in the range 800–1800 cm^{-1} . Although by isotopic substitution of $^{12}\text{CH}_3^{13}\text{C}^{16}\text{O}_2^-$ or $^{13}\text{CH}_3^{13}\text{C}^{16}\text{O}_2^-$ for $^{12}\text{CH}_3^{12}\text{C}^{16}\text{O}_2^-$, the peaks at 1600 and 1320 cm^{-1} shift to 1597 and 1297 cm^{-1} , respectively, they do not shift by isotopic substitution of $^{13}\text{CH}_3^{12}\text{C}^{16}\text{O}_2^-$ for $^{12}\text{CH}_3^{12}\text{C}^{16}\text{O}_2^-$. Thus, $\nu_a(\text{COO})$ and $\nu_s(\text{COO})$ depend on the mass of the carbonyl carbon, but not on the mass of the methyl carbon. Complex **3** with the HCOO^- ligand shows IR spectroscopic features similar to those of **2** with the CH_3COO^- ligand. In the IR spectra of **3** in mineral oil (Figure S2 in Supporting Information), the peaks at 1595 and 1282 cm^{-1} were assigned to $\nu_a(\text{COO})$ and

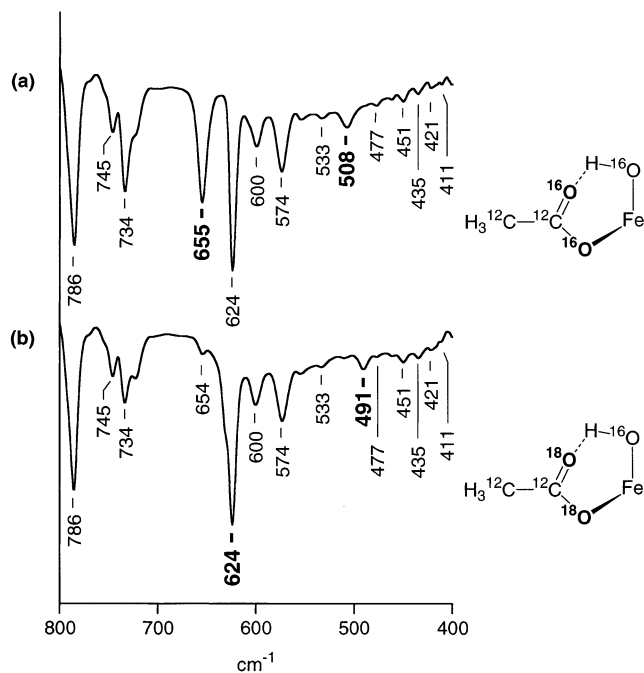


Figure 5. IR spectra in the 400–800 cm^{-1} region in mineral oil of (a) **2** with $^{12}\text{CH}_3^{12}\text{C}^{16}\text{O}_2^-$ and (b) **2** with $^{12}\text{CH}_3^{12}\text{C}^{18}\text{O}_2^-$.

$\nu_s(\text{COO})$, respectively (Table 1). They shift to 1544 and 1261 cm^{-1} , respectively, by isotopic substitution of $\text{H}^{13}\text{C}^{16}\text{O}_2^-$ for $\text{H}^{12}\text{C}^{16}\text{O}_2^-$.

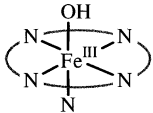
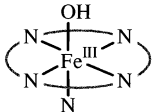
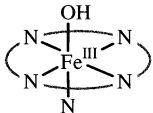
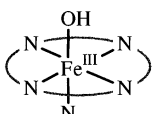
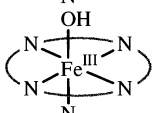
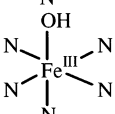
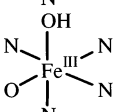
IR Spectra of CC Stretching and OCO Deformation.

In Figure S1 (in Supporting Information), the peak at 908 cm^{-1} was assigned to the C–C stretching of the carboxylato ligands of **2**. It shifts to 905, 900, or 896 cm^{-1} by isotopic substitution of $^{12}\text{CH}_3^{13}\text{C}^{16}\text{O}_2^-$, $^{13}\text{CH}_3^{12}\text{C}^{16}\text{O}_2^-$, or $^{13}\text{CH}_3^{13}\text{C}^{16}\text{O}_2^-$, respectively. Figure 5 shows the IR spectra in mineral oil in the range 400–800 cm^{-1} of **2** with $^{12}\text{CH}_3^{12}\text{C}^{16}\text{O}_2^-$ (spectrum a) and $^{12}\text{CH}_3^{12}\text{C}^{18}\text{O}_2^-$ (spectrum b) ligands. The peak at 655 cm^{-1} (in spectrum a) was assigned to the OCO deformation frequency, $\delta(\text{OCO})$, because the peak shifts to 624 cm^{-1} (in spectrum b) by isotopic substitution of $^{12}\text{CH}_3^{12}\text{C}^{18}\text{O}_2^-$ for $^{12}\text{CH}_3^{12}\text{C}^{16}\text{O}_2^-$. Figure S3 (in Supporting Information) shows the IR spectra of $^{12}\text{CH}_3^{13}\text{C}^{16}\text{O}_2^-$, $^{13}\text{CH}_3^{12}\text{C}^{16}\text{O}_2^-$, and $^{13}\text{CH}_3^{13}\text{C}^{16}\text{O}_2^-$ derivatives of **2** in mineral oil in the range 400–800 cm^{-1} . Although by isotopic substitution of $^{13}\text{CH}_3^{12}\text{C}^{16}\text{O}_2^-$ or $^{13}\text{CH}_3^{13}\text{C}^{16}\text{O}_2^-$ for $^{12}\text{CH}_3^{12}\text{C}^{16}\text{O}_2^-$, the peak at 655 cm^{-1} shifts to 649 and 648 cm^{-1} , respectively, it does not shift by isotopic substitution of $^{12}\text{CH}_3^{13}\text{C}^{16}\text{O}_2^-$ for $^{12}\text{CH}_3^{12}\text{C}^{16}\text{O}_2^-$. Thus, $\delta(\text{OCO})$ depends on the mass of the methyl carbon, but not on that of the carbonyl carbon. In the IR spectra of **3** in mineral oil, the peak at 739 cm^{-1} was assigned to $\delta(\text{OCO})$ (Figure S4 in Supporting Information). It shifts to 732 cm^{-1} by isotopic substitution of $\text{H}^{13}\text{C}^{16}\text{O}_2^-$ for $\text{H}^{12}\text{C}^{16}\text{O}_2^-$.

IR Spectra of COO Rocking. As shown in Table 1, free CH_3COO^- exhibits COO rocking, $\rho_r(\text{COO})$, at 460 cm^{-1} , but free HCOO^- does not exhibit $\rho_r(\text{COO})$.¹⁰ In general, metal–O(carboxylato) stretching, $\nu(\text{M–OCO})$, also appears below 500 cm^{-1} .¹¹ In Figure 5, the peak at 508 cm^{-1} (in spectrum a) shifts to 491 cm^{-1} (in spectrum b) by isotopic substitution of $^{12}\text{CH}_3^{12}\text{C}^{18}\text{O}_2^-$ for $^{12}\text{CH}_3^{12}\text{C}^{16}\text{O}_2^-$. Although

(10) Ito, K.; Bernstein, H. J. *Can. J. Chem.* **1956**, *34*, 170–178.

Table 3. Structural and Spectroscopic Features of Mononuclear Six-Coordinate (Hydroxo)Iron(III) Species

compound	coordination geometry	spin state	λ_{\max} (nm)	$\nu(\text{Fe}^{\text{III}}\text{-OH})$ (cm^{-1})
<i>met</i> -Myoglobin ^a		high-spin (70%)	600, 580, 543	490
<i>met</i> -Hemoglobin ^b		high-spin (45%)	600(sh), 576, 541	495
Horseradish peroxidase ^c		low-spin	605, 575, 543	503 (HRP-C) 516 (HRP A-1)
Cytochrom c peroxidase ^d		low-spin	—	477
[Fe ^{III} (TMPyP)(OH)] ^e		high-spin low-spin	484 (sh)	447 498
DNA-free-Fe ^{III} (bleomycin) ^f		low-spin	385, 365	561
complex 2 ^g		high-spin	527	574

^a Ref 13a,b. pH = 10.2. ^b Ref 13a,c. pH = 10.6. ^c Ref 13d. HRP-C, pH = 12.0; HRP A-1, pH = 10.2. ^d Ref 13e,f. pH = 7.4. ^e Ref 13 g,h. pH = 12.0. TMPyP: tetrakis-5,10,15,20-(2-*N*-methylpyridyl)porphinato. ^f Ref 13i,j. pH = 7.5. ^g This work.

there are two candidates, $\nu(\text{COO})$ and $\nu(\text{Fe-OCO})$, for the peak at 508 cm^{-1} , the candidate $\nu(\text{Fe-OCO})$ is excluded because complex **3** with the HCOO^- ligand does not have any corresponding peaks in this range. Thus, the peak at 508 cm^{-1} in Figure 5a was finally assigned to $\nu(\text{COO})$ of **2**.

IR Spectra of Fe^{III}-OH Stretching. The identification of Fe^{III}-OH stretching frequencies,¹² $\nu(\text{Fe}^{\text{III}}\text{-OH})$, is extremely useful because it directly demonstrates the presence of a particular ligand of the active site. As shown in Table

3, some $\nu(\text{Fe}^{\text{III}}\text{-OH})$ values of mononuclear six-coordinate (hydroxo)iron(III) complexes,¹³ but only one example for non-heme enzyme,^{13i,j} have been reported. In these cases, the structures have not been characterized by X-ray crystallographic analysis. Figure 6 shows the IR spectra of $^{18}\text{OH}^-$ (spectrum b), $^{16}\text{OD}^-$ (spectrum c), and $^{18}\text{OD}^-$ (spectrum d) derivatives of **2** in mineral oil in the range $480\text{--}610\text{ cm}^{-1}$. The peak at 574 cm^{-1} (in spectrum a) was assigned to the $\nu(\text{Fe}^{\text{III}}\text{-}^{16}\text{OH})$ that shifts to 554 cm^{-1} (in spectrum b) by isotopic substitution of $^{18}\text{OH}^-$ for $^{16}\text{OH}^-$ (Table 2). The shift value (-20 cm^{-1}) is about 80% that expected by Hooke's law calculations for a pure Fe^{III}-O stretching mode (-25 cm^{-1}). Intriguingly, $\nu(\text{Fe}^{\text{III}}\text{-OH})$ does not depend on the mass of the hydroxo hydrogen; that is, $\nu(\text{Fe}^{\text{III}}\text{-OH})$ does

- (11) Although there are many references on vibrational spectra of metal complexes of carboxylic acids, amino acids, and related ligands, only a very few of them give assignments on metal-O(carboxylato) vibrations. (a) Bourke, J. P.; Cannon, R. D.; Grinter, R.; Jayasooriya, U. A. *Spectrochim. Acta* **1993**, *49A*, 685–690. (b) Gau, H.-M.; Chen, C.-T.; Jong, T.-T.; Chien, M.-Y. *J. Organomet. Chem.* **1993**, *448*, 99–106. (c) Pal, S.; Gohdes, J. W.; Willisch, W. C. A.; Armstrong, W. H. *Inorg. Chem.* **1992**, *31*, 713–716. (d) Inomata, Y.; Shibata, A.; Yukawa, Y.; Takeuchi, T.; Moriwaki, T. *Spectrochim. Acta* **1988**, *44A*, 97–107. (e) Straughan, B. P.; Moore, W.; McLaughlin, R. *Spectrochim. Acta* **1986**, *42A*, 451–456. (f) Süß-Fink, G.; Herrmann, G.; Morys, P. *J. Organomet. Chem.* **1985**, *284*, 263–273. (g) Deacon, G. B.; Phillips, R. J. *Coord. Chem. Rev.* **1980**, *33*, 227–250. (h) Kincaid, J. R.; Nakamoto, K. *Spectrochim. Acta* **1976**, *32A*, 277–283. (i) Condrate, R.; Nakamoto, K. *J. Chem. Phys.* **1965**, *42*, 2590–2598.
- (12) (a) Kitagawa, T.; Ogura, T. *Prog. Inorg. Chem.* **1997**, *45*, 4431–479. (b) Kitagawa, T.; Mizutani, Y. *Coord. Chem. Rev.* **1994**, *135/136*, 685–735. (c) Kurtz, D. M., Jr. *Chem. Rev.* **1990**, *90*, 585–606. (d) Shiemke, A. K.; Loehr, T. M.; Sanders-Loehr, J. *J. Am. Chem. Soc.* **1986**, *108*, 2437–2443.

- (13) (a) Asher, S. A.; Schuster, T. M. *Biochemistry* **1979**, *18*, 5377–5387. (b) Desbois, A.; Lutz, M.; Banerjee, R. *Biochemistry* **1979**, *18*, 1510–1518. (c) Asher, S. A.; Vickery, L. E.; Schuster, T. M.; Sauer, K.; *Biochemistry* **1977**, *16*, 5849–5856. (d) Sitter, A. J.; Shifflett, J. R.; Turner, J. J. *Biol. Chem.* **1988**, *263*, 13032–13038. (e) Han, S.; Ching, Y.-C.; Rousseau, D. L. *Nature* **1990**, *348*, 89–90. (f) Han, S.; Ching, Y.-C.; Rousseau, D. L. *J. Biol. Chem.* **1989**, *264*, 6604–6607. (g) Reed, R. A.; Rodgers, K. R.; Kushmeider, K.; Spiro, T. G.; Su, Y. O. *Inorg. Chem.* **1990**, *29*, 2881–2883. (h) Rodgers, K. R.; Reed, R. A.; Spiro, T. G. *New J. Chem.* **1992**, *16*, 533–535. (i) Sam, J. W.; Takahashi, S.; Lippai, I.; Peisach, J.; Rousseau, D. L. *J. Biol. Chem.* **1998**, *273*, 16090–16097. (j) Takahashi, S.; Sam, J. W.; Peisach, J.; Rousseau, D. L. *J. Am. Chem. Soc.* **1994**, *116*, 4408–4413.

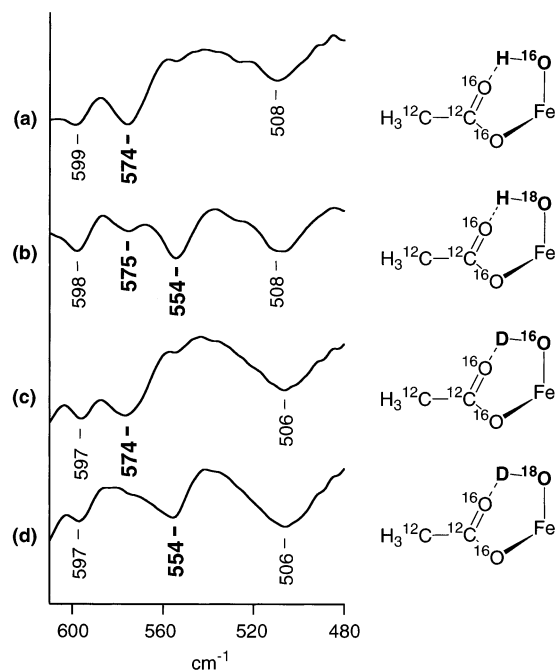


Figure 6. IR spectrum in the 480–610 cm^{-1} region in mineral oil of (a) **2** with $^{16}\text{OH}^-$, (b) **2** with $^{18}\text{OH}^-$, (c) **2** with $^{16}\text{OD}^-$, and (d) **2** with $^{18}\text{OD}^-$.

not shift by isotopic substitution of $^{16}\text{OD}^-$ for $^{16}\text{OH}^-$ or $^{18}\text{OD}^-$ for $^{18}\text{OH}^-$. This is attributed to the weak Fe–O–H bending force constant that should be influenced by the strength of the $\text{Fe}^{\text{III}}\text{--O--H}\cdots\text{O}(\text{carboxylato})$ hydrogen bond.¹⁴ The IR spectra in mineral oil of **3** (Figure S5 in Supporting Information) indicate the same tendency of the spectra in mineral oil of **2**. The IR spectra in acetonitrile of **2** and **3** indicate the same tendency of their spectra in mineral oil (Figure S6 in Supporting Information). Borovik et al.^{9a} have reported that the five-coordinate (oxo)iron(III) complex displays a $\nu(\text{Fe}^{\text{III}}\text{--}^{16}\text{O})$ at 671 cm^{-1} that is markedly higher than the value (574 cm^{-1}) of $\nu(\text{Fe}^{\text{III}}\text{--}^{16}\text{OH})$ of the six-coordinate (hydroxo)iron(III) complexes **2** and **3**.

IR Spectra of $\text{Fe}^{\text{III}}\text{OH}$ Deformation and OH Stretching.

Nakamoto has revealed that metal complexes containing the hydroxo group exhibit $\delta(\text{MOH})$ in the range 700–1200 cm^{-1} .¹⁵ Spiro et al. have reported that the $\delta(\text{Fe}^{\text{III}}\text{OH})$ of a sterically hindered porphyrin is calculated to be 614 cm^{-1} for FeOH and 437 cm^{-1} for FeOD species.^{13g} Unfortunately, complexes **2** and **3** do not show any H/D isotope sensitive peaks that can be assigned to $\delta(\text{Fe}^{\text{III}}\text{OH})$ in the range 400–1200 cm^{-1} . The IR spectrum of **2** shows the OH vibration at 3277 cm^{-1} which shifts to 3273 cm^{-1} with added H_2^{18}O .⁷

ESI Mass Spectra. It was confirmed by ESI-MS that the structures of **1–3** are preserved in acetonitrile under the same conditions of IR experiments in acetonitrile. Figure 7a shows the positive ion mass spectrum of **2** showing prominent signals at m/z 677.6 (relative intensity (I) = 100% in the range m/z 100–2000) and m/z 617.4 (I = 95%). The signal

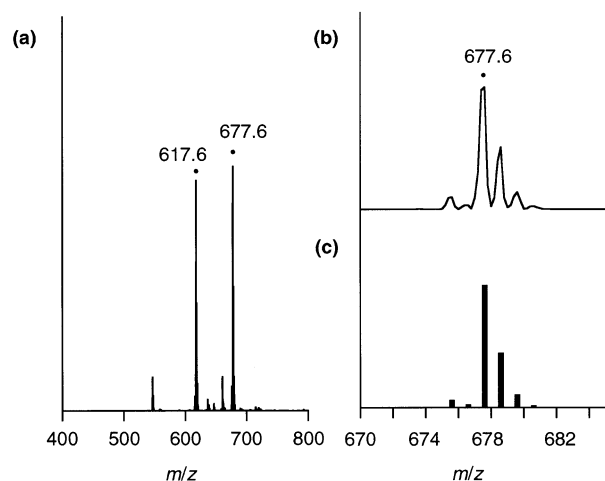


Figure 7. (a) Positive ion ESI mass spectrum of **2** in acetonitrile. The signal at m/z 677.6 corresponds to $[\mathbf{2} - \text{ClO}_4]^+$; that at m/z 617.6 is a product ion of $[\mathbf{2} - \text{ClO}_4]^+$. (b) Signal at m/z 677.6. (c) Calculated isotopic distribution for $[\mathbf{2} - \text{ClO}_4]^+$.

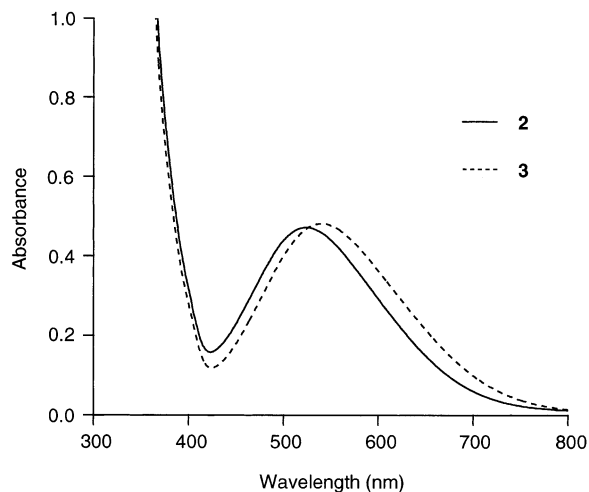


Figure 8. UV–vis spectra of acetonitrile solutions of **2** (—) and **3** (---) at ambient temperature.

at m/z 677.6 has a characteristic distribution of isotopomers that matches well with the calculated isotopic distribution for $[\text{Fe}(\text{TNPA})(\text{OH})(\text{CH}_3\text{CO}_2)]^+$ ($[\mathbf{2} - \text{ClO}_4]^+$, Figure 7b,c). It is determined by MS/MS measurements that the signal at m/z 617.4 is a product ion ($[\mathbf{2} - \text{ClO}_4 - \text{CH}_3\text{CO}_2\text{H}]^+$) of $[\mathbf{2} - \text{ClO}_4]^+$.

UV–Vis and EPR Spectra. Acetonitrile solutions of **1–3** exhibit UV–vis spectra with distinct bands at 536 nm ($\epsilon = 1000\text{ M}^{-1}\text{ cm}^{-1}$), 527 nm ($\epsilon = 1200\text{ M}^{-1}\text{ cm}^{-1}$, Figure 8), and 538 nm ($\epsilon = 1300\text{ M}^{-1}\text{ cm}^{-1}$, Figure 8), respectively. The EPR spectra of **1** (Figure S7a in Supporting Information), **2** (Figure 9), and **3** (Figure S7b) in acetonitrile at 77 K show typical axial signals of high-spin iron(III) at $g_{\perp} = 6.00$ and $g_{\parallel} = 2.00$ for **1**, $g_{\perp} = 5.99$ and $g_{\parallel} = 1.99$ for **2**, and $g_{\perp} = 6.00$ and $g_{\parallel} = 2.00$ for **3**. The E/D values of **1**, **2**, and **3** are 0.00, 0.01, and 0.00, respectively.¹⁶ These values agree well with the E/D value (0.01, axial) of the plant LO (SLO-1),^{17,18} which is quite different from the E/D values (0.32 and 0.33, rhombic) of the mammalian LOs (15-RLO and human 15-LO; 15-HLO, respectively).^{18,19} Our model more closely resembles the coordination environment of the mammalian

(14) There is no effect of H/D substitution (OH/OD substitution) on $\nu_a(\text{COO})$ and $\nu_s(\text{COO})$.

(15) Nakamoto, K. In *Infrared and Raman Spectra of Inorganic and Coordination Compounds Part B: Applications in Coordination, Organometallic, and Bioinorganic Chemistry*, 5th ed.; John Wiley & Sons: New York, 1997; pp 57, 274.

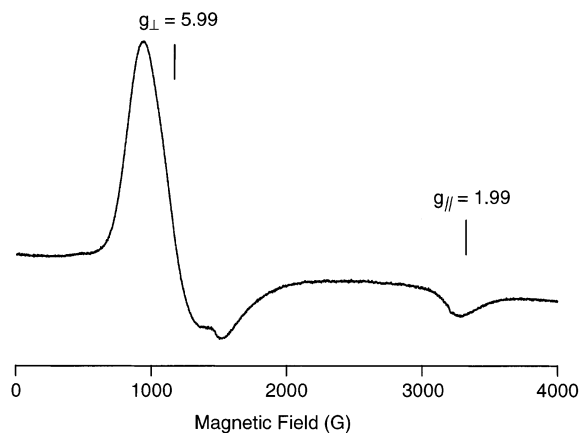


Figure 9. EPR spectrum of an acetonitrile solution of **2** at 77 K.

LOs, yet the EPR of our model resembles the axial signal of the plant LO. This result may challenge our current understanding of the lipoxygenase EPR, because Solomon et al. have proposed an explanation of the axial signal in the plant LO and the rhombic signal in the mammalian LOs.¹⁸ The high-spin iron(III) ($S = 5/2$) state of complex **1** was confirmed by the magnetic susceptibility measurement at 297 K, giving $\mu_{\text{eff}} = 5.9 \mu_{\text{B}}$ (with an estimated maximal error of $\pm 10\%$)⁷ which is close to the expected value: $5.92 \mu_{\text{B}}$ ($= 2[S(S+1)]^{1/2}$). Borovik et al.⁹ have reported that the five-coordinate (oxo)iron(III) complex is axial but the five-coordinate (hydroxo)iron(III) complex is more rhombic.

Electrochemical Measurements. Complexes **1–3** exhibit quasireversible cyclic voltammetric waves of $\text{Fe}^{3+}/\text{Fe}^{2+}$ couples in acetonitrile at ambient temperature with $E^{\circ}_{1/2}$ (vs SCE) = -0.09 V ($\Delta E = 0.11$ V, Figure S8a in Supporting Information), -0.20 V ($\Delta E = 0.08$ V, Figure 10), and -0.10 V ($\Delta E = 0.09$ V, Figure S8b), respectively, which are much lower than the reduction potential (0.36 V vs SCE = 0.60 V vs NHE)²⁰ of the plant LO (SLO-1). This result may suggest that the reduction potential of the mammalian LOs (15-RLO/HLO) is lower than that of SLO-1 because our model more closely approaches the ligand field of the mammalian LOs, even though the synthetic ligand is different from the protein coordination environment. Solomon et al. have reported that the structural changes observed in the spectroscopies of SLO-1 and 15-RLO/HLO can strongly affect the reduction potentials (E° of SLO-1 $> E^{\circ}$ of 15-

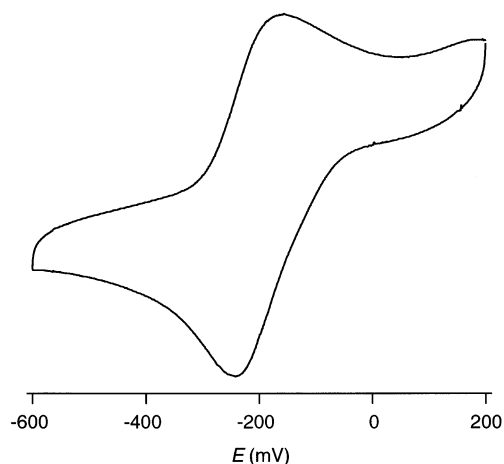


Figure 10. Cyclic voltammogram wave of an acetonitrile solution of **2** at ambient temperature.

RLO/HLO) and hence the catalytic rate (k_{cat} of SLO $> k_{\text{cat}}$ of 15-HLO).^{1a} Borovik et al.^{9b} have reported that the five-coordinate (hydroxo)iron(II) complex exhibits a cyclic voltammogram wave of $\text{Fe}^{3+}/\text{Fe}^{2+}$ couple in *N,N*-dimethylformamide with $E^{\circ}_{1/2}$ (vs SCE) = -1.40 V that is lower than the values of **1–3**.

Conclusions

We have reported detailed characterization of the *cis* (hydroxo)- Fe^{III} -(carboxylato) configuration of mononuclear six-coordinate (hydroxo)iron(III) complexes, $[\text{Fe}^{\text{III}}(\text{tnpa})(\text{OH})(\text{RCO}_2)]\text{ClO}_4$ [**1**, R = C_6H_5 ; **2**, R = CH_3 ; **3**, R = H] as model complexes for the proposed (hydroxo)iron(III) species of LOs. The *cis* (hydroxo)- Fe^{III} -(carboxylato) configuration favors a formation of an intramolecular hydrogen bond between the hydroxo and the carboxylato ligands. Isotopic labeling experiments show that the intramolecular hydrogen bond considerably reflects the IR spectra of the *cis* (hydroxo)- Fe^{III} -(carboxylato) unit.

Experimental Section

Caution! The perchlorate salts in this study are all potentially explosive and should be handled with care.

Materials and Methods. Isotopomers H_2^{18}O (95% ^{18}O), D_2^{16}O (99% D), D_2^{18}O (99% D and 95% ^{18}O), $^{12}\text{CH}_3^{12}\text{C}^{18}\text{ONa}$ (95% ^{18}O), $^{12}\text{CH}_3^{13}\text{C}^{16}\text{O}_2\text{Na}$ (99% ^{13}C), $^{13}\text{CH}_3^{12}\text{C}^{16}\text{O}_2\text{Na}$ (99% ^{13}C), $^{13}\text{CH}_3^{13}\text{C}^{16}\text{O}_2\text{Na}$ (99% ^{13}C), and $\text{H}^{13}\text{C}^{16}\text{O}_2\text{Na}$ (99% ^{13}C) were purchased from Isotec Co. Ltd. Infrared spectra were recorded on a Nicolet AVATAR 360 FT-IR instrument using 2 cm^{-1} standard resolution at ambient temperature. Mass data were obtained by an API 300 triple quadrupole mass spectrometer (PE-Sciex) equipped with ESI interfaces. The sprayer was held at a potential of +4.5 kV for positive ion detection mode, and compressed N_2 was employed to assist liquid nebulization. Orifice potential was maintained at +25 V. Visible spectra were obtained on an Otsuka MCPD-2000 spectrometer. EPR spectra were obtained at X-band on a JEOL JES-RE1X spectrometer at 77 K under nonsaturating microwave power conditions. The magnitude of modulation was chosen to optimize the resolution and signal-to-noise (S/N) ratio of the observed spectra. The g values were calibrated with a Mn^{2+} marker. Electrochemical measurements were performed in a 10^{-3} M acetonitrile solution with 10^{-1} M (*n*-Bu)₄NBF₄ as a supporting

- (16) The E/D value defines the rhombicity of the ligand field. High-spin iron(III) with axial symmetry: $E/D = 0.00$. High-spin iron(III) with rhombic symmetry: $E/D = 0.33$. The E/D value of high-spin iron(III) was evaluated from EPR g values (when $g_x - g_y < 2$): $g_x = 6 + 24(E/D) - 79(E^2/D^2)$, $g_y = 6 - 24(E/D) - 79(E^2/D^2)$, and $g_z = 2 - 34(E^2/D^2)$. See: Palmer, G. *Biochem. Soc. Trans.* **1985**, *13*, 548–560.
- (17) (a) Slappendel, S.; Veldink, G. A.; Vliegthart, J. F. G.; Aasa, R.; Malmström, B. G. *Biochim. Biophys. Acta* **1981**, *667*, 77–86. (b) Groot, J. J. M. C.; Garssen, G. J.; Veldink, G. A.; Vliegthart, J. F. G.; Boldingh, J.; Egmond, M. R. *FEBS Lett.* **1975**, *56*, 50–54.
- (18) We appreciate the reviewer's comment about the relevance of our EPR results to Solomon's work: (a) Holman, T. H.; Zhou, J.; Solomon, E. I. *J. Am. Chem. Soc.* **1998**, *120*, 12564–12572. (b) Zhang, Y.; Gan, Q. F.; Pavel, E. G.; Sigal, E.; Solomon, E. I. *J. Am. Chem. Soc.* **1995**, *117*, 7422–7427.
- (19) Carroll, R. T.; Muller, J.; Grimm, J.; Dunham, W. R.; Sands, R. H.; Funk, M. O., Jr. *Lipids* **1993**, *28*, 241–244.
- (20) Nelson, M. J. *Biochemistry* **1988**, *27*, 4273–4278.

electrolyte on a BAS660A electrochemical analyzer using a Pt working electrode at 25 °C. Under these conditions, the Fc^+/Fc (ferrocenium/ferrocene) couple lies at +0.418 V versus SCE. The potentials of $E^{\circ}_{1/2}$ are the average values of anodic and cathodic peak potentials in cyclic voltammograms recorded at 100 mV s^{-1} .

[Fe^{III}(tnpa)(OH)(C₆H₅CO₂)]ClO₄ (1). C₆H₅CO₂Na (2.64 mg, 18.3 μmol) dissolved in H₂O (20 μL) was added to an acetonitrile solution (2.0 mL) of Fe(ClO₄)₃·6H₂O (8.50 mg, 18.3 μmol) and tnpa (10.0 mg, 18.3 μmol). After stirring for 5 h, the solution was concentrated giving purple powder of **1**, which was collected by filtration, washed with a small amount of diethyl ether, and dried in vacuo (yield: 20%). Anal. Calcd for C₄₀H₆₀N₇O₈ClFe (**1**·H₂O): C, 55.98; H, 7.05; N, 11.42. Found: C, 56.06; H, 6.94; N, 11.42.

[Fe^{III}(tnpa)(OH)(CH₃CO₂)]ClO₄ (2). The procedures for making **1** were followed. Anal. Calcd for C₃₅H₅₆N₇O_{7.5}ClFe (**2**·0.5H₂O): C, 53.47; H, 7.18; N, 12.47. Found: C, 53.39; H, 7.24; N, 12.47.

[Fe^{III}(tnpa)(OH)(HCO₂)]ClO₄ (3). The procedures for making **1** were followed. Anal. Calcd for C₃₄H₅₃N₇O₇ClFe (**3**): C, 53.51; H, 7.00; N, 12.85. Found: C, 53.24; H, 6.90; N, 12.98.

X-ray Crystallographic Analysis. Crystallographic data for **1**⁷ and **2** have been deposited with the Cambridge Crystallographic Data Center as supplementary publication no. CCDC-101084 and 158545, respectively. Copies of the data can be obtained free of charge on application to CCDC, 12 Union Road, Cambridge

CB21EZ, U.K. [Fax(+44)1223-336-033. E-mail: deposit@ccdc.cam.ac.uk.] Purple crystals of **2** used in X-ray analysis were obtained by diffusion of diethyl ether into an acetonitrile solution of **2**. Measurements for **2** were made on a Rigaku/MSC Mercury CCD diffractometer with graphite monochromated Mo K α radiation ($\lambda = 0.7107 \text{ \AA}$). Calculations were performed using the teXsan crystallographic software package of Molecular Structure Corporation. Crystal data, data collection parameters, structure solution and refinement, atomic coordinates, anisotropic displacement parameters, bond lengths, and bond angles of **2** are given in Supporting Information.

Acknowledgment. Financial support of this research by the Ministry of Education, Science, and Culture Grant-in-Aid for Scientific Research to S.O. (13640568) and Y.W. (11490036 and 11228208) is gratefully acknowledged. We thank Prof. K. Nakamoto (Marquette University) and Dr. Y. Mizutani (Institute for Molecular Science) for valuable discussions.

Supporting Information Available: IR, EPR, and CV spectra and crystallographic information. This material is available free of charge via the Internet at <http://pubs.acs.org>.

IC0200040